Role of Steric Stabilization on the Arrested Growth of Silver Nanocrystals in Supercritical Carbon Dioxide

Parag S. Shah, Shabbir Husain, Keith P. Johnston, and Brian A. Korgel*

Department of Chemical Engineering and Texas Materials Institute, Center for Nano- and Molecular Science and Technology, The University of Texas, Austin, Texas 78712-1062

Received: May 24, 2002; In Final Form: September 7, 2002

Perfluorodecanethiol-stabilized silver (Ag) nanocrystals were synthesized in supercritical (sc)-CO_2 through arrested precipitation, by reducing silver acetylacetonate (Ag(acac)) with hydrogen in the presence of fluorinated thiol. The CO_2 density used during synthesis controls the particle size and polydispersity. At high solvent densities, ($P > 250$ bar, $T = 80$ °C), the ligands provide a strong steric barrier that maintains small particles with a 20 Å diameter. At lower solvent densities ($P < 250$ bar, $T = 80$ °C), the osmotic repulsions between capping ligands are weak, resulting in 40 Å diameter nanocrystals with higher polydispersity. At early stages in the growth process, metal core coagulation competes with ligand adsorption. Conditions effective for steric stabilization, such as long ligands and high solvent density, quench nanocrystal growth at relatively low ligand binding densities, which leads to smaller nanocrystals. Under poor solvent conditions, particles grow to larger sizes before the coverage of capping ligand is sufficient to prevent coagulation of metal particles. Perfluorodecanethiol-coated silver nanocrystals, synthesized in either good or poor solvent conditions, readily redisperse in acetone, fluorinated solvents, and sc-CO_2 (at high density). The precursor concentration, thiol: precursor ratio, and reaction time do not affect the nanocrystal size appreciably, although these parameters do affect the polydispersity.

Introduction

Nanocrystals ranging from 20 to 100 Å in diameter represent a unique class of colloids, capable of exhibiting a variety of size-dependent optical and electronic properties that could be used in a variety of technologies, including coatings, environmental, chemical processing, medical, electronic, and sensing applications.[1−3] To effectively utilize their size-dependent properties, the nanocrystal size and polydispersity must be controlled. For this purpose, organic stabilizing ligands with proper binding strengths for the substrate[4−6] are often used to passivate the nanocrystal surfaces and quench particle growth.[2] The ligands determine the particle dispersibility and enable postsynthesis separation techniques, such as antisolvent-based size selective precipitation. After the solvent is evaporated, the stabilizing ligands control the edge-to-edge separation between the metal cores and permit redispersion. In some cases, the capping ligands can affect the nanocrystal shape.[7]

Recently, nanocrystals have been synthesized in supercritical fluids (SCFs).[8−11] SCFs provide a unique reaction medium with density tunable solvation properties, which in some cases can be exploited to manipulate nanocrystal and nanowire morphology through temperature and pressure changes in the reaction medium.[12,13] Nanocrystal dispersibility in SCFs can be tuned as well, since the ligand−solvent interaction strength, which is responsible for colloid stabilization, relates directly to the solvent density.[14,15] Supercritical carbon dioxide (sc-CO_2) provides a potentially useful environment for nanocrystal synthesis, as it is nontoxic, nonflammable, and environmentally benign. However, the low polarizability per volume of CO_2 gives rise to weak van der Waals forces and sterically stabilized systems in sc-CO_2 require "CO_2-philic" groups with low cohesive energy densities to provide favorable energetic interactions with the solvent.[16−19] Although examples of colloids stabilized by hydrocarbon surfactants in sc-CO_2 exist,[20,21] generally, fluorinated groups are needed.[22,23] To minimize solvation challenges, several groups have now utilized water-in-CO_2 microemulsions as nanoreactors for synthesizing various types of nanocrystals.[8,9] However, these approaches yield particles with weakly bound surfactants and the resulting nanocrystals cannot be collected without irreversible flocculation; the CdS nanocrystals developed by Holmes et al. are an exception to this case.[8] Recently, we showed that silver nanocrystals capped with partially fluorinated ligands (1H,1H,2H,2H-perfluorodecanethiol) are redispersible in sc-CO_2.[24] Subsequently, we demonstrated arrested precipitation in pure CO_2 using hydrogen to reduce an organometallic precursor[25] in the presence of fluorinated ligands (1H,1H,2H,2H-perfluorooctanethiol);[10] however, the particles formed in these studies were relatively large (∼55 Å) and very polydisperse (∼47%). Furthermore, although these nanocrystals were well-capped with the ligand and dispersed in acetone, the nanocrystals did not redisperse in sc-CO_2, as their chain lengths were too short to overcome the relatively strong van der Waals attraction between metal particles of this size in sc-CO_2.

Herein, we reveal that longer chain lengths (1H,1H,2H,2H-perfluorodecanethiol; C_{10} vs C_8) produce small nanocrystals, 20 Å in diameter with 37% polydispersity under good solvent conditions (i.e., high CO_2 density). The nanocrystal size and polydispersity depend sensitively on the supercritical solvent conditions. Low solvent density yields large nanocrystals with

* To whom correspondence should be addressed. Tel: (512)471-5633. Fax: (512)471-7060. E-mail: korgel@mail.che.utexas.edu.

10.1021/jp026180b CCC: $22.00
Published on Web 11/05/2002

very broad size distributions. The size and size distribution of the nanocrystals synthesized under "poor" solvent conditions match those obtained earlier[10] using the shorter C_8 stabilizing ligands at high CO_2 density. These observations are consistent with the model for nanocrystal steric stabilization presented in ref 14. High ligand capping density provides a thick steric barrier that prevents metal core coagulation under both good and poor solvent conditions. However, strong osmotic repulsions between ligands in good solvent conditions slow nanocrystal growth at a much lower capping density. Long ligands and high solvent density produce small nanocrystals; ineffective stabilization at low CO_2 density leads to larger more polydisperse nanocrystals. Our model for particle coagulation as a function of ligand binding density reveals that relatively low ligand surface coverages dramatically slow coagulation under conditions providing effective steric stabilization.

Experimental Section

Materials. The silver precursor, silver acetylacetonate (Ag(acac), Aldrich Chemical Co.), 1H,1H,2H,2H-perfluorodecanethiol (Oakwood Products Inc.), heptane (Aldrich Chemical Co.), and Omnisolve spectrophotometry grade acetone (EM Science) were used as received. High-grade carbon dioxide (purity >99.99%, Matheson Gas Products) and hydrogen (purity >99.999%, Praxair Inc.) were used.

Nanocrystal Synthesis. In a typical experiment, 12−15 mg of Ag(acac) was loaded into the front of a variable volume view cell. The front of the cell was filled with pressurized liquid CO_2 (138 bar and 21 °C) using a manual pressure generator (High Pressure Equipment Corp.) until reaching the desired precursor concentration. CO_2 was added into the back of the cell using a computer-controlled syringe pump (Dionex model 501) to increase the system pressure. The system was heated by wrapping the cell with heating tape attached to an Omega CN76000 temperature controller. Once the cell reached the desired reaction conditions, 1H,1H,2H,2H-perfluorodecanethiol and hydrogen were added to the cell through two injection loops attached in series to the front of the cell. Injection loops of various lengths were used to control the volume of added thiol from 7.6 to 150 μL. The hydrogen pressure was varied from 21 to 69 bar in an 800 μL injection loop to maintain a fixed hydrogen:precursor concentration of 30:1. Typical reaction times were 3 h. Then, the cell was cooled and depressurized by venting the CO_2 from the back of the cell. CO_2 was slowly vented from the front of the cell, leaving only the nanocrystals, excess thiol, and reaction byproducts. The nanocrystals were collected from the cell using acetone. To remove reaction byproducts and excess thiol, heptane was added as an antisolvent to precipitate the nanocrystals, which were subsequently isolated by centrifugation. The nanocrystals could then be redispersed in acetone, sc-CO_2, or fluorinated solvents (Fluorinert or Freon).

Transmission Electron Microscopy (TEM). High-resolution TEM images were obtained using a JEOL 2010F microscope with 1.4 Å point-to-point resolution equipped with a GATAN digital photography system for imaging and operating with a 200 kV accelerating voltage. Low-resolution TEM images were acquired on a Phillips EM280 microscope with a 4.5 Å point-to-point resolution operating with an 80 kV accelerating voltage. For imaging, the nanocrystals were deposited from acetone onto 200 mesh carbon-coated copper TEM grids. Average particle size and polydispersity were determined using Scion Image for Windows software. At least 300 nanocrystals were measured to determine the average nanocrystal size, standard deviation, the arithmetic mean radius, $r_1 = \sum r_i/N_\infty$, cube mean radius, $r_3 = 3/\sqrt{\sum r_i^3/N_\infty}$, and harmonic mean radius, $r_h = N_\infty/\sum (1/r_i)$, where N_∞ is the total number of particles. The moments of the size distribution, $\mu_1 = r_3/r_h$ and $\mu_3 = r_1/r_3$, were determined from these measurements.

UV−Visible Absorbance Spectroscopy. UV−visible absorbance spectra were measured in a high-pressure optical cell equipped with sapphire windows on opposing sides with an optical path length of 0.9 cm with a 1.75 cm aperture. The cell was loaded with nanocrystals by evaporating a drop of an acetone dispersion into the cell. CO_2 was slowly added to the cell using a computer-controlled syringe pump (ISCO Corp.) until reaching the desired pressure. An inline ball check valve (High Pressure Equipment Corp.) was used to prevent nanocrystal diffusion back into the pump. The cell was wrapped with heating tape connected to an Omega CN76000 temperature controller. The absorbance measurements were acquired on a Beckman DU-40 UV−vis spectrophotometer at 1 nm intervals from 200 to 800 nm. It was not feasible to measure spectra during reaction due to the absorbance of the organic moieties in the precursor.

Perfluorodecanethiol Cloud Point Measurements. The solubility of perfluorodecanethiol in sc-CO_2 was determined using a high-pressure variable volume view cell equipped with a front-facing sapphire window. Initially, 1 mL of perfluorodecanethiol was added to the cell. The thiol concentration was controlled by the addition of CO_2 to the cell using a computer-controlled syringe pump (ISCO Corp.). After the desired concentration was reached, the cell was pressurized to 172 bar by filling the back of the cell with CO_2. The temperature was controlled by immersing the cell into an 80 °C water bath. After the cell equilibrated, it was depressurized at ~7 bar/min until reaching the cloud point. The cloud point was defined as the pressure at which the piston was no longer visible. Cloud point determinations were repeated three times for accuracy. Carbon dioxide was then added to the front of the cell to dilute the thiol concentration, and the process was repeated.

Results

Perfluorodecanethiol-stabilized silver nanocrystals were synthesized at 80 °C in sc-CO_2 by reducing Ag(acac) with hydrogen at a variety of precursor and thiol concentrations and pressures. The reaction conditions explored in this study are summarized in Table 1. The nanocrystals were generally well-passivated by the ligands. They redisperse in acetone and fluorinated solvents such as freon and fluorinert, which are good solvents for the ligands. The TEM images show distinct particles separated by the adsorbed ligands. For example, the perfluorodecanethiol-coated silver nanocrystals in Figure 1 are separated by an average edge-to-edge distance of 21 Å. This interparticle separation is larger than what is found for hydrocarbon-stabilized nanocrystals (decanethiol gives ~12.5 Å[26]), due to the increased stiffness of the fluorinated ligand.[27] The lattice spacing in the high-resolution TEM images in Figure 1 of 2.3 Å corresponds to the d_{111} spacing in silver.

The significant finding in this paper is the distinct dependence of the nanocrystal size and polydispersity on the solvent density during particle formation. Well-passivated silver nanocrystals could be synthesized at a wide range of solvent pressures, from 207 to 345 bar. However, they do not redisperse at pressures less than 276 bar (at 80 °C)—as observed in the UV−visible absorbance spectra in Figure 2. Figure 3 shows the size and polydispersity of nanocrystals synthesized at 80 °C, 3.5 mM

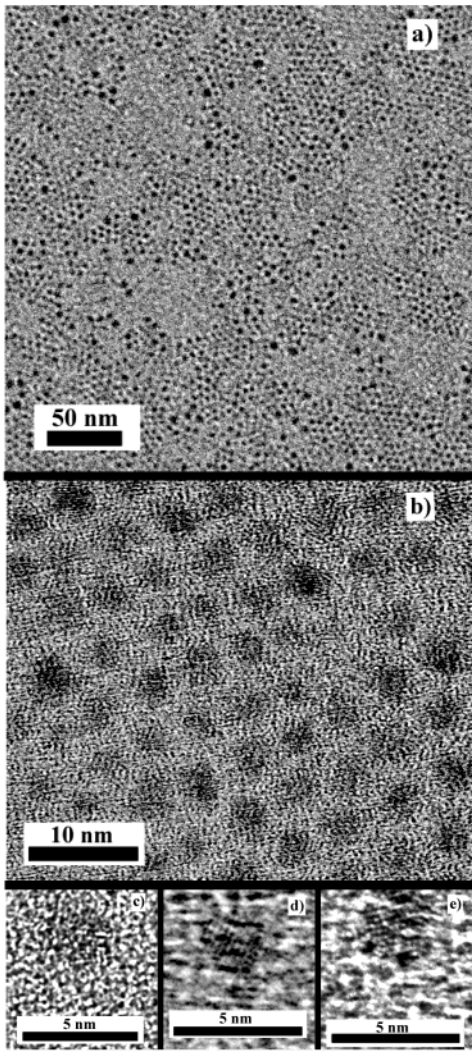

Figure 1. Representative TEM images of silver nanocrystals capped with perfluorodecanethiol synthesized in sc-CO_2. Panels a and b show images of nanocrystals grown at 80 °C and 276 bar (experiment B), which have formed rafts of close packed particles. Panels c−e show high-resolution TEM images exhibiting crystalline cores.

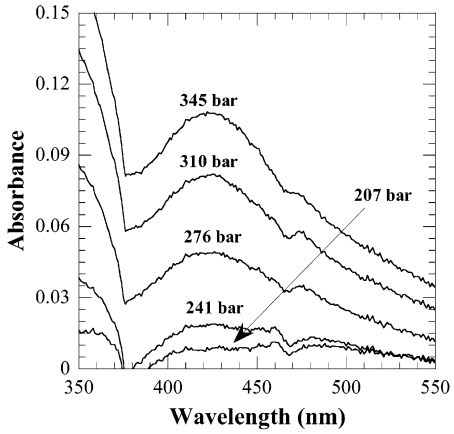

Figure 2. UV−visible absorbance measurements of silver nanocrystals dispersed in sc-CO_2 at 80 °C and pressures of 207, 241, 276, 310, and 345 bar. The decrease in peak intensity with decreased pressure indicates reduced solubility of the particles.

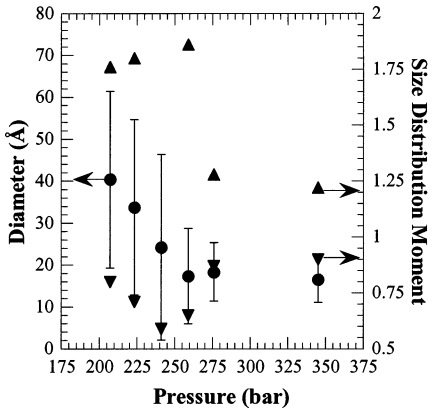

Figure 3. Data points correspond to experiments A−F. (a) Average nanocrystal diameter (●) and size distribution moments, μ_1 (▲) and μ_3 (▼), of perfluorodecanethiol-coated silver nanocrystals synthesized at 80 °C, with a precursor concentration of 3.5 mM and thiol:precursor ratio of 2.5 as a function of solvent pressure. The error bars represent the standard deviation of the samples. μ_1 for experiment D (3.1) has not been shown for clarity.

Ag(acac), and thiol:precursor ratio of 2.5. Above 276 bar, the particles exhibit an average diameter of 20 Å and the synthesis pressure does not noticeably affect the nanocrystal size or polydispersity. However, below 276 bar, both the nanocrystal size and the polydispersity increase with decreasing pressure (Figure 4). Nanocrystals synthesized below the dispersibility limit of 276 bar are still well-passivated by the ligands and redisperse in acetone, fluorinated solvents, and sc-CO_2 at 80 °C and pressures greater than 276 bar.

TABLE 1: Summary of the Conditions Used for Nanocrystal Growth

exp no.	prec concn (mM)	thiol/prec ratio (mol/mol)	temp (°C)	pressure (bar)	density (g/mL)	reaction time (h)	avg diameter (Å)	standard deviation (Å)	% standard deviation	μ_1	μ_3
A	3.5	2.4	80	345	0.786	3	17	6	33	1.2	0.9
B	3.5	2.5	80	276	0.720	3	18	7	38	1.3	0.9
C	3.4	2.4	80	259	0.698	3	17	11	66	1.9	0.7
D	3.5	2.3	80	241	0.674	3	24	22	91	3.1	0.6
E	3.5	2.6	80	223	0.643	3	34	21	62	1.8	0.7
F	3.5	2.5	80	207	0.610	3	40	21	52	1.8	0.8
G	0.8	2.6	80	276	0.720	3	19	4	21	1.1	1.0
H	1.8	2.5	80	276	0.720	3	12	4	34	1.3	0.9
I	0.9	2.2	80	207	0.610	3	27	14	51	1.5	0.8
J	1.7	2.5	80	207	0.610	3	27	18	65	1.8	0.7
K	3.5	2.4	80	276	0.720	6	17	15	92	2.6	0.6
L	3.5	2.5	80	276	0.720	12	18	11	61	1.8	0.7
M	3.5	0.3	80	276	0.720	3	18	7	37	1.3	0.9
N	3.4	0.5	80	276	0.720	3	12	4	37	1.3	0.9
O	3.5	4.9	80	276	0.720	3	14	6	39	1.3	0.9
P	3.5	5.0	80	276	0.720	3	20	10	52	1.5	0.8

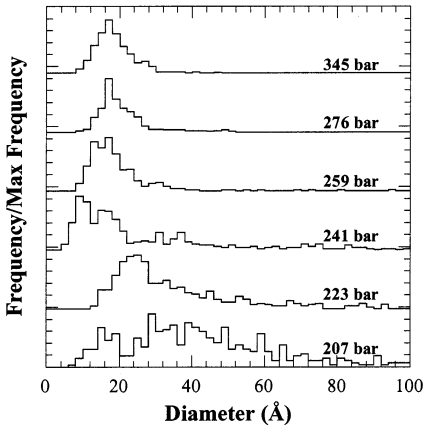

Figure 4. Data points correspond to experiments A−F. Particle size distributions as a function of solvent density. The size distribution histograms have been normalized (frequency/max frequency) and offset for clarity.

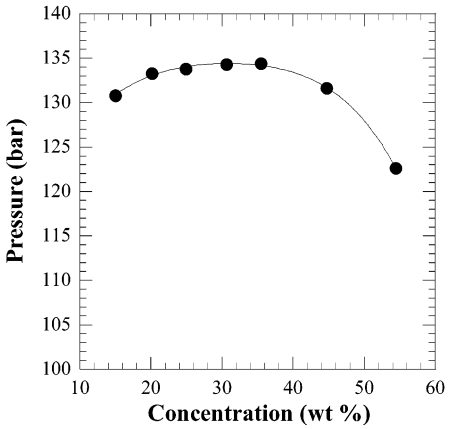

Figure 5. Cloud point measurements of perfluorodecanethiol in sc-CO_2 at 80 °C.

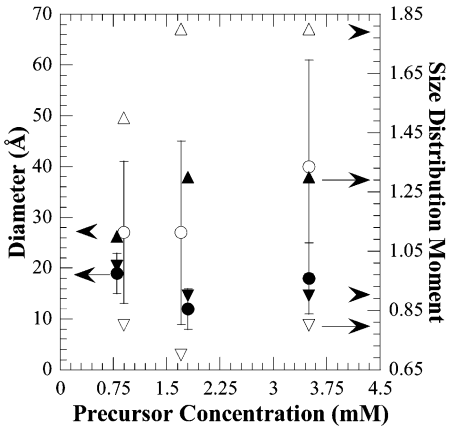

Figure 6. Average diameter (●) and size distribution moments, μ_1 (▲) and μ_3 (▼), of perfluorodecanethiol-stabilized silver nanocrystals grown at 80 °C with a thiol:precursor ratio of 2.5:1, as a function of precursor concentration. The closed symbols correspond to 276 bar and experiments B, G, and H, while the open symbols correspond to 207 bar and experiments F, I, and J. The error bars represent the standard deviation of the samples.

The size distribution moments, μ_1 and μ_3, reflect the particle growth mechanism. Nanocrystals formed through condensation of free atoms, or small oligomers, onto growing metal cores are relatively monodisperse with $\mu_1 = \mu_3 = 1$, whereas coagulative growth results in broad size distributions with $\mu_1 > 1.25$ and $\mu_3 < 0.905$.[28] The size distribution moments indicate that particles grow by coagulation at pressures below 276 bar.[29] Above 276 bar, μ_1 and μ_3 approach 1, revealing that growth occurs through a combination of both coagulation and condensation. These results indicate that high solvent density slows particle aggregation, which largely prevents coagulation and stabilizes particles in the small size range. At lower solvent density, where ligand solvation is poor, particles grow primarily by coagulation.

Because colloid stability is provided by the adsorbed ligands, understanding ligand solvation is very important. As particles collide, well-solvated ligands repel each other through osmotic forces. To stabilize the nanocrystal dispersion, these forces must overcome the long range attraction between particles due to van der Waals forces. For colloids in conventional solvents, which exhibit upper critical solution temperatures (UCST), good and bad solvent regions are defined by the θ temperature, which relates to the critical flocculation temperature. Analogously, colloids in SCFs exhibit lower critical solution temperatures (LCST), and the strength of the steric repulsion is most closely related to the density of the solvent.[30,31] The cohesive energy density of the solvent is higher at increased solvent density, resulting in better ligand−solvent interactions.[16] In SCFs, the critical flocculation density (CFD) defines the solvent conditions where the dispersion is no longer stable. Monte Carlo simulations have shown that the CFD in SCFs corresponds to the density where the stabilizer ligand is soluble at all concentrations, defined as the upper critical solution density (UCSD).[32−34] The UCSD for perfluorodecanethiol in sc-CO_2 was determined to be ∼135 bar at 80 °C, as shown in Figure 5. Figure 2, however, reveals that pressures greater than ∼276 bar are required for nanocrystal stabilization, indicating that the CFD does not correspond to the UCSD. It is important to note that the simulation results in ref 34 do not account for colloidal core−core attractions, which are relatively strong for metal nanocrystals. For polydisperse systems, the CFD can be blurred, due to the fact that larger particles have stronger core−core attractions than smaller particles.[14] As shown in Figure 2, the absorbance peak is greatest at the highest pressure, indicating that the most nanocrystals have dispersed in CO_2.[35] The peak height decreases as the pressure is lowered, indicating that the largest nanocrystals have flocculated at that condition. As the pressure decreases below 276 bar, the absorbance disappears altogether, as the steric repulsion has become so weak that none of the particles are stabilized at this condition.

At good solvent conditions, 276 bar, and 80 °C, the reaction time and thiol:precursor ratio do not affect the average nanocrystal size. Increased reaction time simply leads to a slight broadening of the particle size distribution, perhaps as the result of Ostwald ripening (see Supporting Information, Figures 1S and 2S). Therefore, the reaction times studied here were limited to 3 h. The thiol:precursor ratio could be varied widely, from 1:3 to 5:1 (thiol:precursor mole ratio), with little effect on the nanocrystal size and size distribution (Supporting Information, Figure 3S). The thiol:precursor ratio needed for total surface coverage of 20 Å diameter silver nanocrystals, assuming an average area per thiol of 16 Å^2, is approximately 1:3.[2,26] Thiol diffusion to the nanocrystal surface does not appear to be size-limiting.

The precursor concentration, however, can affect the nanocrystal size and size distribution. Under poor solvent conditions, both the size and the polydispersity are affected. Under good solvent conditions, only the size distribution appears affected by the precursor concentration—higher precursor concentration leads to broader size distributions. Figure 6 plots the particle

size and polydispersity for nanocrystals synthesized under poor solvation conditions. As the precursor concentration increases, μ_1 and μ_3 deviate increasingly from 1, signifying that these conditions favor coagulation. A higher precursor concentration increases the initial concentration of silver nuclei, which increases collision rates at early times in the growth process. At lower solvent density, an increased precursor concentration results in larger nanocrystals as the number of initial collisions increases. The size distribution moments indicate that coagulative growth is greater at lower pressure for all precursor concentrations.

Discussion

On the basis of the fact that μ_1 and μ_3 deviate significantly from 1 under all of the reaction conditions studied, nanocrystal coagulation is clearly an important growth mechanism to understand. Coagulative nanocrystal growth requires interparticle collisions that bring the metal cores close enough to promote metal fusion.[36] Particles with complete ligand surface coverage do not fuse because the metal cores are sterically prevented from touching—even in a poor solvent (or no solvent for that matter). Therefore, almost certainly at very early times in the particle formation process, nanocrystals are only partially coated with ligands in order for coagulation to occur. To gain an appreciation for the combined influences of ligand surface coverage and solvent strength on the growth process, the coagulation rate between particles can be calculated. On the basis of the obvious influence of coagulation, it is assumed that at very early times in the particle formation process, nanocrystals will be only partially coated with ligands and particle coagulation will compete with ligand adsorption. Although the ligand adsorption rate or ligand binding constants between thiols and silver in sc-CO_2 are unknown, the coagulation rate between particles can be calculated with respect to particle size, solvent strength, and ligand surface coverage in order to better understand the growth process.

The nanocrystal coagulation rate (J_{12}) of particles of size "1" with particles of size "2" depends on their initial concentrations, N_1 and N_2: $J_{12} = K_{12}N_1N_2$.[37] K_{12} is the coagulation coefficient. Considering the simplest case when particle collisions occur through Brownian motion, $K_{12} = K_{12}^{\text{Brownian}} = 4\pi(R_1 + R_2)(D_1 + D_2)$. The cluster diffusivities, D_i, can be estimated using the Stokes−Einstein equation, $D_i = kT/6\pi\mu R_i$, where k is Boltzmann's constant, T is the temperature, and μ is the CO_2 viscosity. For equally sized silver particles in sc-CO_2 at 80 °C and 276 bar, $K_{12}^{\text{Brownian}} = 2.2 \times 10^{-10}$ cm^3/sec. Note that K_{12}^{Brownian} is independent of the core radius when equally sized particles are considered. Attractive or repulsive interactions with energy $\Phi(x)$, where x is the center-to-center separation distance, affect the collision rate and must be accounted for using a correction factor W:[37]

$$W = (R_1 + R_2)\int_{R_1+R_2}^{\infty} \exp\left(\frac{\Phi(x)}{kT}\right)x^{-2}\,dx \qquad (1)$$

Subsequently, $K_{12} = K_{12}^{\text{Brownian}}/W$.

The van der Waals interaction between two equally sized particles of radius R depends on the Hamaker constant, A_{121}, for silver acting across CO_2:[36]

$$\Phi_{\text{vdW}} = -\frac{A_{121}}{6}\left[\frac{2R^2}{x^2-4R^2} + \frac{2R^2}{x^2} + \ln\left(\frac{x^2-4R^2}{x^2}\right)\right] \qquad (2)$$

A_{121} relates directly to the Hamaker constants for CO_2 and silver across vacuum, A_{11} and A_{22}, respectively; $A_{121} \approx (\sqrt{A_{11}} - \sqrt{A_{22}})^2$. A_{22} has been determined to be 2.2 eV.[36] A_{11} can be determined using equations of state for the density-dependent dielectric constant, ϵ_1, and refractive index, n_1, for CO_2[38] and Lifshitz theory:[36,39]

$$A_{11} = \frac{3}{4}kT\left(\frac{\epsilon_1 - 1}{\epsilon_1 + 1}\right)^2 + \frac{3h\nu_e}{16\sqrt{2}}\frac{(n_1^2 - 1)^2}{(n_1^2 + 1)^{3/2}} \qquad (3)$$

In eq 3, h is Planck's constant and ν_e is the maximum electronic ultraviolet adsorption frequency, typically assumed to be 3×10^{15} s^{-1}. The Hamaker constant for silver across sc-CO_2 at 276 bar and 80 °C is 1.5 eV.[36] Taking $A_{121} = 1.5$ eV, $W = 0.71$ to give $K_{12} = K_{12}^{\text{Brownian}}/W = 3.1 \times 10^{-10}$ cm^3/sec.

Of course, sterically stabilized nanocrystals undergo many collisions without coagulation and particle growth. Therefore, steric stabilization must be properly accounted for to determine the coagulation rate. As a general guideline, the metal cores fuse if they approach to within 5 Å (δ_c) of each other.[36] Because the interparticle separation for perfluorodecanethiol-coated nanocrystals in the absence of solvent is 21 Å, well-passivated nanocrystals are protected from fusion and coagulative growth under all solvent conditions. Partially passivated nanocrystals, however, have the possibility of fusing into larger clusters if the cores approach to within δ_c upon collision. Early in the growth process, particle coagulation competes with ligand adsorption. Therefore, to prevent coagulative nanocrystal growth—which leads to large particle sizes and polydispersity—the solvent must enable the ligands to fully extend and prevent cluster coagulation between partially capped cores until capping becomes sufficiently high. The repulsive force between particles provided by the ligands can be included in W using a model for steric stabilization.

Vincent et al. proposed that steric interactions between particles result from osmotic and elastic repulsions.[40,41] The osmotic repulsive energy (Φ_{osm}) results from the unfavorable exclusion of solvent between colliding nanocrystals, and the elastic term evolves from the mechanical compression of the layer that prevents the metal cores from touching. Φ_{osm} depends on the particle radius R and the center-to-center separation distance x:

$$\Phi_{\text{osm}} = \frac{4\pi R k_b T}{\upsilon_{\text{solv}}}\phi^2\left(\frac{1}{2} - \chi\right)\left(l - \frac{x-2R}{2}\right)^2 \quad l < d - 2R < 2l \qquad (4)$$

$$\Phi_{\text{osm}} = \frac{4\pi R k_b T}{\upsilon_{\text{solv}}}\phi^2\left(\frac{1}{2} - \chi\right)\left[l^2\left(\frac{x-2R}{2l} - \frac{1}{4} - \ln\left(\frac{x-2R}{l}\right)\right)\right] \quad d - 2R < l \qquad (5)$$

In eqs 4 and 5, υ_{solv} is the molecular volume of the solvent and ϕ is the volume fraction profile of the stabilizer extending from the particle surface. Important parameters in eqs 4 and 5 include the ligand length, l, and the Flory−Huggins interaction parameter, χ, between the ligand and the solvent. In Flory−Huggins theory, $\chi = 1/2$ typically represents the boundary between a good solvent ($\chi < 1/2$) and a poor solvent ($\chi > 1/2$). Φ_{osm} can be significant even at low surface coverage of ligand in a good solvent. When $\chi > 1/2$, Φ_{osm} becomes attractive due to the poor solubility of the ligands. To determine solvent conditions in SCFs, the compressibility must be accounted for and effective (density-dependent) χ parameters can be used.[42,43] For sc-CO_2, however, the density dependence of χ is not well-known.

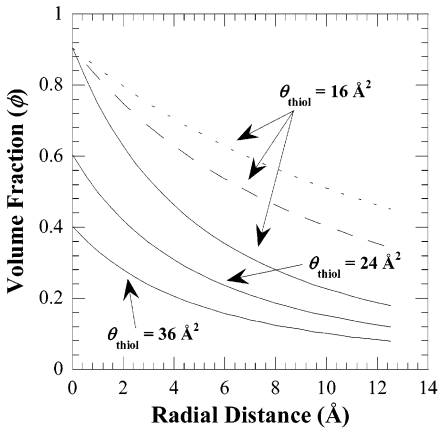

Figure 7. Ligand volume fraction profiles as a function of radial distance from particle surface. Particle sizes shown are 20 Å diameter (—), 40 Å diameter (- - -), and 60 Å in diameter (· · ·) at full surface coverage $\theta_{thiol} = 16$ Å^2. Also shown are volume fraction profiles for 20 Å nanocrystals at varying surface coverages, $\theta_{thiol} = 16$ Å^2, $\theta_{thiol} = 24$ Å^2, and $\theta_{thiol} = 36$ Å^2.

Therefore, in the analysis presented here, χ parameters simply provide guidelines for understanding how good, θ, and poor solvent conditions affect particle growth, rather than providing an explicit relationship to the CO_2 density. Although more sophisticated models have been developed for solvent−tail interactions in SCFs to include effects of compressibility,[32−34] the simpler model presented below captures many of the key features needed to explain the trends in coagulation rates in this paper.

The volume fraction profile (ϕ) of the stabilizing ligands decreases radially from the metal surface and depends on the particle size and "footprint" area per headgroup. The radial decay of the volume fraction profile increases with decreasing particle size due to the increased interfacial curvature, as shown in Figure 7. The ϕ curves in Figure 7 were calculated using the geometric equation for cylinders with ligand cross-section area (SA_{thiol}) of 14.5 Å,[226] extending radially from a curved surface with radius $R_p + z$:

$$\phi(z) = \frac{SA_{thiol}R_p}{\theta_{thiol}(R_p + z)} \tag{6}$$

where θ_{thiol} is the surface area per thiol headgroup, which represents the binding density, and z is the radial distance from the metal surface. Coagulation rates are plotted as a function of the ligand volume fraction at the metal surface, $\phi_s = \phi_{z=0}$ in Figures 8 and 9, taking the close-packed layer to have a density of 16 Å^2/thiol.[26]

Low molecular weight alkane and fluoroalkane stabilizers undergo only a very slight amount of compression, as the only ligand mobility is rotation around a few carbon−carbon bonds. For this reason, the elastic term given by Vincent is not applicable; instead, a modified hard sphere model is used to represent the repulsion due to high packing density of thiol on the nanocrystal surface. The metal surfaces of colliding particles cannot approach closer than a minimum separation distance x_{msd}, at which point the ligand volume fraction in the interfacial region, ϕ_{total}, reaches 1. The volume fraction profile in the interfacial region is determined by using the volume fraction profiles of opposing particles at a given separation distance, determined using eq 6, and adding the volume fractions in the region of ligand overlap. x_{msd} can be thought of as an effective hard sphere separation distance between colliding particles.

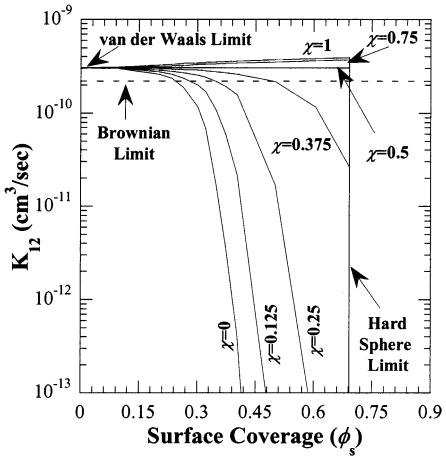

Figure 8. K_{12} for 20 Å diameter perfluorodecanethiol-stabilized silver nanocrystals as a function of thiol surface coverage (ϕ_s) at varying solvent conditions (χ). Solvent conditions shown are $\chi = 0$, 0.125, 0.25, 0.375, 0.5 (θ), 0.75, and 1.0. Brownian limit corresponds to the coagulation coefficient determined without any interparticle interactions (2.2×10^{-10} cm^3/sec). The van der Waals limit corresponds to the coagulation coefficient with the incorporation of interparticle van der Waals attractions (3.1×10^{-10} cm^3/sec), without any steric effect from the ligand. The hard sphere limit is the surface coverage necessary to prevent core fusion (separation distance > 5 Å).

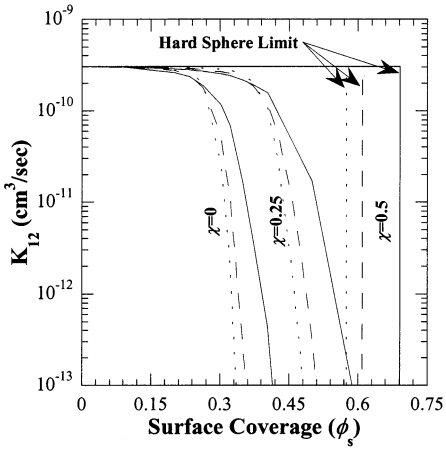

Figure 9. Coagulation coefficient (K_{12}) as a function of thiol surface coverage (ϕ_s) at varying particle sizes, 20 Å diameter (—), 40 Å diameter (- - -), and 60 Å diameter (· · ·). Solvent conditions shown are $\chi = 0$, 0.25, and 0.5 (θ). The hard sphere limits correspond to the surface coverage needed to prevent core fusion (separation distance > 5 Å).

Figure 7 shows that x_{msd} increases with higher binding density and increasing diameter. If the metal cores approach to within the critical fusion distance δ_c, they will fuse. If $x_{msd} \geq \delta_c$, nanocrystal aggregation will not lead to fusion and the coagulative growth will stop. The ligand surface coverage (ϕ_s) when this occurs in a θ solvent ($\chi = 1/2$) is called the hard sphere limit, denoted as $\phi_{s,HS}$. Note that even at poor solvent conditions, the hard sphere repulsion provided by the adsorbed ligand can protect the cores from fusion. Notice in Figure 9 that $\phi_{s,HS}$ decreases with increasing particle diameter. In other words, θ_{thiol} at the hard sphere limit for coagulation is considerably less for larger particles than for smaller particles.

Figure 8 shows K_{12} calculated for 20 Å diameter perfluorodecanethiol-stabilized silver nanocrystals as a function of ϕ_s by inserting $\Phi_{total} = \Phi_{vdw} + \Phi_{osm}$ into eq 1. In a good solvent ($\chi < 1/2$), K_{12} decreases as ϕ_s increases due to the improved steric barrier between nanocrystals. When $\chi = 1/2$, $\Phi_{osm} = 0$ and K_{12} does not depend on ϕ_s until reaching the hard sphere

limit at $\phi_{s,HS} = 0.69$. Note that at complete coverage $\phi_s = 0.91$. When $\chi > 1/2$, the poorly solvated ligands increase the interparticle attractions and K_{12} increases with higher ϕ_s, until reaching the hard sphere limit when coagulative growth stops. At all solvent conditions, nanocrystal coagulation terminates at the hard sphere limit. However, nanocrystal growth in a good solvent terminates at ligand surface coverages significantly lower than $\phi_{s,HS}$. The ϕ_s amount required to prevent particle coagulation increases significantly as the solvent quality decreases due to the loss of osmotic repulsion between the nanocrystals. Under ideal solvent conditions ($\chi = 0$), coagulative nanocrystal growth is quenched at $\phi_s = 0.41$.

Figure 9 shows K_{12} calculated as a function of nanocrystal size and solvent condition. The value of ϕ_s necessary to stop nanocrystal growth is lower for larger nanocrystals for all χ. For example, in a $\chi = 0$ solvent, 20 Å particles require a surface coverage of $\phi_s = 0.41$, while 60 Å particles require only $\phi_s = 0.34$. Larger particles exhibit less surface curvature than smaller particles, which enhances the steric repulsion between particles.

Consistent with the nanocrystal absorbance spectra in Figure 2, χ decreases as the solvent density increases. In fact, the system is below the CFD at the lowest pressures. Therefore, provided that ligand binding rates do not vary significantly with pressure, nanocrystal coagulation terminates earlier in the growth process when using higher pressures, thus leading to smaller particles with lower polydispersity.

In ref 10, silver nanocrystals were synthesized in CO_2 using perfluorooctanethiol (C_8) as a capping ligand. The particles were relatively large and polydisperse and did not redisperse in CO_2, even at high density. At a precursor concentration of 3.5 mM, the average particle diameter was 57 ± 28 Å (polydispersity of ~47%) for perfluorooctanethiol, while it was only 16 ± 6 Å (polydispersity of 39%) for perfluorodecanethiol. $\mu_1 = 1.5$ and $\mu_3 = 0.8$ for the particles coated with perfluorooctanethiol, as compared to values of $\mu_1 = 1.3$ and $\mu_3 = 0.9$ for the particles capped with perfluorodecanethiol. The C_8 chains are much less effective as a steric stabilizer as compared with the C_{10} chains, and particle coagulation dominates growth when using the shorter chains. The transition from coagulation-dominated particle growth to controlled growth and stabilization of particles in the small size range occurs when going from low CO_2 density to high CO_2 density and from increasing the ligand chain length from C_8 to C_{10}. For example, when osmotic steric stabilization is lost at a reaction pressure of 207 bar, the average particle diameter increases to 40 ± 21 Å, which is much closer to the sizes synthesized in ref 10. The longer ligand, which also has a greater ratio of CF_2 to CH_2 groups, is more effective at preventing coagulative collisions between particle cores. However, fully passivated cores are protected from irreversible flocculation even at conditions where the ligand cannot provide dispersibility—consider, for example, the deposited nanocrystals in the TEM images and the fact that well-capped nanocrystals of all sizes can be flocculated and precipitated using antisolvents without irreversible coagulation or change in nanocrystal size.[3,26] These results show the importance of steric stabilization during the growth stage on maintaining control over particle size and polydispersity.

Conclusions

Silver nanocrystals have been synthesized in sc-CO_2 by reducing a CO_2 miscible organometallic precursor with hydrogen in the presence of perfluorodecanethiol capping ligands. The ligands effectively bind to the nanocrystal surface, allowing them to be collected, cleaned, and redispersed in acetone, fluorinated solvents, and sc-CO_2. The unique density tunable solvation characteristics of SCFs provide a means to examine the effect of steric stabilization on the arrested precipitation of nanocrystals.

At high solvent densities, the ligands are adequately solvated and capable of preventing coagulative collisions between growing clusters with relatively low ligand surface coverage. The resulting nanoparticles are in the range of 20 Å. Decreasing the solvent pressure to conditions where the ligands are no longer capable of stabilizing the nanocrystals causes the average particle size to increase significantly. The growth mechanism becomes coagulation-dominated, and a much higher ligand surface coverage is needed to provide the thick steric layer necessary to prevent fusion between metal cores. Coagulation during the time it takes to achieve this higher surface coverage results in larger particles with higher polydispersity. The large differences for silver nanocrystal size and redispersibility for the perfluorooctanethiol vs perfluorodecanethiol ligand result from the improved steric stabilization provided by the latter. In addition to solvent quality, other parameters typically found to affect particle size were examined. In contrast with our previous study with perfluorooctanethiol,[10] the average particle size is independent of precursor concentration under good solvent conditions. Lowering the thiol:precursor ratio does not increase the particle size, indicating that thiol diffusion to the nanocrystal surface is rapid. The influence of effective ligand stabilization as described by the experimental data and model in this study should be universal for all single-phase nanocrystal synthesis, even in conventional solvents.

Acknowledgment. This work is supported in part by the STC Program of the National Science Foundation under Agreement No. CHE-9876674 and the Welch Foundation. B.A.K. also thanks NSF (Agreement No. CTS-9984396) for support through a CAREER Award.

Supporting Information Available: Full description of the materials. This material is available free of charge via the Internet at http://pubs.acs.org.

References and Notes

(1) Alivisatos, A. P. *Science* **1996**, *271*, 933−937.

(2) Brust, M.; Walker, M.; Bethell, D.; Schiffrin, D. J.; Whyman, R. *J. Chem. Soc., Chem. Commun.* **1994**, *7*, 801−802.

(3) Murray, C. B.; Norris, D. J.; Bawendi, M. G. *J. Am. Chem. Soc.* **1993**, *115*, 8706−8715.

(4) Sun, S.; Murray, C. B. *J. Appl. Phys.* **1999**, *85*, 4325−4330.

(5) Sun, S.; Murray, C. B.; Weller, D.; Folks, L.; Moser, A. *Science* **2000**, *287*, 1989−1992.

(6) The functional group that binds to the metal has a dramatic impact on the nanocrystal size. The binding must be strong enough to induce ligand sticking; however, binding must be sufficiently reversible to allow for particle growth. Various metals require a mixture of capping ligands to achieve these properties. For example, FePt nanocrystals require a mixture of oleic acid and oleylamine (ref 5) while Co nanocrystal growth requires a mixture of oleic acid and alkyl phosphines (ref 4).

(7) Puntes, V. F.; Krishnan, K. M.; Alivisatos, A. P. *Science* **2001**, *291*, 2115−2117.

(8) Holmes, J. D.; Bhargava, P. A.; Korgel, B. A.; Johnston, K. P. *Langmuir* **1999**, 6613−6615.

(9) Ohde, H.; Hunt, F.; Wai, C. M. *Chem. Mater.* **2001**, *13*, 4130−4135.

(10) Shah, P. S.; Husain, S.; Johnston, K. P.; Korgel, B. A. *J. Phys. Chem. B* **2001**, *105*, 9433−9440.

(11) Cason, J. P.; Roberts, C. B. *J. Phys. Chem. B* **2000**, *104*, 1217−1221.

(12) Holmes, J. D.; Johnston, K. P.; Doty, R. C.; Korgel, B. A. *Science* **2000**, *287*, 1471.

(13) Ziegler, K. J.; Doty, R. C.; Johnston, K. P.; Korgel, B. A. *J. Am. Chem. Soc.* **2000**, *123*, 7797−7803.

(14) Shah, P. S.; Holmes, J. D.; Johnston, K. P.; Korgel, B. A. *J. Phys. Chem. B* **2002**, *106*, 2545−2551.
(15) Clarke, N. Z.; Waters, C.; Johnson, K. A.; Satherly, J.; Schiffrin, D. J. *Langmuir* **2001**, *17*, 6048−6050.
(16) O'Neill, M. L.; Cao, Q.; Fang, M.; Johnston, K. P.; Wilkinson, S. P.; Smith, C. D.; Kerschner, J. L.; Jureller, S. H. *Ind. Eng. Chem. Res.* **1998**, *37*, 3067−3079.
(17) O'Shea, K.; Kirmse, K.; Fox, M. A.; Johnston, K. P. *J. Phys. Chem.* **1991**, *95*, 7863.
(18) McClain, J. B.; Londono, D.; Combes, J. R.; Romack, T. J.; Canelas, D. A.; Betts, D. E.; Wignal, G. D.; Samulski, E. T.; DeSimone, J. M. *J. Am. Chem. Soc.* **1996**, *118*, 917−918.
(19) Hoefling, T. A.; Beitle, R. R.; Enick, R. M.; Beckman, E. J. *Fluid Phase Equilib.* **1993**, *83*, 203−212.
(20) Johnston, K. P.; Cho, D.; Ryoo, W.; Psathas, P. A.; DaRocha, S. R. P.; Webber, S. E.; Eastoe, J.; DuPont, A.; Steytler, D. C. *Langmuir* **2001**, *17*, 7191−7193.
(21) Sarbu, T.; Styranec, T.; Beckman, E. J. *Nature* **2000**, *405*, 165−168.
(22) Johnston, K. P.; Harrison, K. L.; Clarke, M. J.; Howdle, S. M.; Heitz, M. P.; Bright, F. V.; Carlier, C.; Randolph, T. W. *Science* **1996**, *271*, 624.
(23) DeSimone, J. M.; Maury, E. E.; Menceloglu, Y. Z.; McClain, J. B.; Romack, T. J.; Combes, J. R. *Science* **1994**, *265*, 356.
(24) Shah, P. S.; Holmes, J. D.; Doty, R. C.; Johnston, K. P.; Korgel, B. A. *J. Am. Chem. Soc.* **2000**, *122*, 4245−4246.
(25) Previously, high quality thin films have been formed by using a hybrid chemical fluid deposition (CFD) technique in which organometallic precursors dissolved in sc-CO_2 are reduced by hydrogen. (a) Watkins, J. J.; Blackburn, J. M.; McCarthy, T. J. *Chem. Mater.* **1999**, *11*, 213−215. (b) Blackburn, J. M.; Long, D. P.; Cabañas, A.; Watkins, J. J. *Science* **2001**, *294*, 141−145.
(26) Korgel, B. A.; Fullam, S.; Connolly, S.; Fitzmaurice, D. *J. Phys. Chem. B* **1998**, *102*, 8379−8388.
(27) Chidsey, C. E. D.; Loiacono, D. N. *Langmuir* **1990**, *6*, 682−691.
(28) Pich, J.; Friedlander, S. K.; Lai, F. S. *Aerosol Sci.* **1970**, *1*, 115−126.
(29) Nanocrystals in this size range that form via coagulation still exhibit crystalline cores, as internal lattice reorientation occurs readily in metal particles to eliminate energetically unfavorable crystallographic mismatches. (a) Miki-Yoshida, M.; Tehuacanero, S.; Jose-Yacaman, M. *Surf. Sci. Lett.* **1992**, *274*, L569−L576. (b) Jose Yacaman, M.; Ascencio, J. A.; Liu, H. B.; Gardea-Torresdey, J. *J. Vac. Sci. Technol., B* **2001**, *19*, 1091−1103.
(30) Calvo, L.; Holmes, J. D.; Yates, M. Z.; Johnston, K. P. *J. Supercrit. Fluids* **2000**, *16*, 247−260.
(31) Yates, M. Z.; Shah, P. S.; Johnston, K. P.; Lim, K. T.; Webber, S. *J. Colloid Interface Sci.* **2000**, *227*, 176−184.
(32) Meredith, J. C.; Johnston, K. P. *Macromolecules* **1998**, *31*, 5507−5517.
(33) Meredith, J. C.; Johnston, K. P. *Macromolecules* **1998**, *31*, 5518−5528.
(34) Meredith, J. C.; Sanchez, I. C.; Johnston, K. P.; de Pablo, J. J. *J. Chem. Phys.* **1998**, *109*, 6424−6434.
(35) Bohren, C. F.; Huffman, D. R. *Absorption and Scattering of Light by Small Particles*; John Wiley & Sons: New York, 1983.
(36) Israelachvili, J. *Intermolecular & Surface Forces*, 2nd ed.; Academic Press: San Diego, 1992.
(37) Seinfeld, J. H. *Atmospheric Chemistry and Physics of Air Pollution*; John Wiley & Sons: New York, 1986.
(38) Lewis, J. E.; Biswas, R.; Robinson, A. G.; Maroncelli, M. *J. Phys. Chem. B* **2001**, *105*, 3306−3318.
(39) Hamaker, H. C. *Physica* **1937**, *4*, 1058−1072.
(40) Vincent, B.; Luckham, P. F.; Waite, F. A. *J. Colloid Interface Sci.* **1980**, *73*, 508−521.
(41) Romero-Cano, M. S.; Puertas, A. M.; de la Nieves, F. J. *J. Chem. Phys.* **2000**, *112*, 8654−8659.
(42) Croucher, M. D.; Hair, M. L. *Macromolecules* **1978**, *11*, 874−879.
(43) Croucher, M. D.; Hair, M. L. *J. Phys. Chem.* **1979**, *83*, 1712−1717.